

State of stress in the Southern Tyrrhenian subduction zone from fault-plane solutions

A. Frepoli, G. Selvaggi, C. Chiarabba and A. Amato

Istituto Nazionale di Geofisica, Via di Vigna Murata 605, 00143 Rome, Italy

Accepted 1996 January 30. Received 1996 January 12; in original form 1995 July 31

SUMMARY

In this paper we present revised locations and original focal mechanisms computed for intermediate and deep earthquakes that occurred within the Southern Tyrrhenian subduction zone between 1988 and 1994, in order to improve our knowledge of the state of stress for this compressional margin. In particular, we define the stress distribution within a large portion of the descending slab, between 40 and about 450 km depth. The seismicity distribution reveals a continuous 40–50 km thick slab that abruptly increases its dip from subhorizontal in the Ionian Sea to a constant 70° dip in the Tyrrhenian. We computed focal mechanisms for events with magnitudes ranging from 2.7 and 5.7, obtaining the distribution of *P*- and *T*-axes for many events for which centroid moment tensor (CMT) solutions are not available, thus enabling the sampling of a larger depth range compared to previous studies. We define three portions of the slab characterized by different distributions of *P*- and *T*-axes. A general down-dip compression is found between 165 and 370 km depth, whereas in the upper part of the slab (40–165 km depth) the fault-plane solutions are strongly heterogeneous. Below 370 km the *P*-axes of the few deep events located further to the north have a shallower dip and are not aligned with the 70° dipping slab, possibly suggesting that they belong to a separated piece of subducted lithosphere. There is a good correspondence between the depth range in which the *P*-axes plunge closer to the slab dip (~70°) and the interval characterized by the highest seismic energy release (190–370 km).

Key words: deep focus earthquakes, fault-plane solutions, Southern Tyrrhenian, subduction.

INTRODUCTION

The Southern Tyrrhenian subduction zone (STSZ) is part of the complex geodynamic pattern of the Mediterranean region, arising from collision between the African and Eurasian plates due to N–S- to NNW–SSE-directed convergence over the past 70 Myr (Dewey *et al.* 1973; Dercourt *et al.* 1986; Philip 1987). The STSZ is characterized by crustal, intermediate, and deep seismicity with high seismic energy release (Ritsema 1979; Gasparini *et al.* 1982; Anderson & Jackson 1987; Giardini & Velonà 1991). The main features characterizing this geodynamically active region (Fig. 1) are the subduction of the Ionian oceanic lithosphere beneath the Calabrian Arc (Malinverno & Ryan 1986; Patacca & Scandone 1989; Royden, Patacca & Scandone 1987; Doglioni 1991; Selvaggi & Chiarabba 1995), the recent (post-Tortonian) opening of the Tyrrhenian basin (Barberi *et al.* 1978) driven by back-arc migration (Malinverno & Ryan 1986), the high heat flow of the Tyrrhenian basin (Hutchison *et al.* 1983), the present

uplift of the Calabrian Arc (Westaway 1993; Miyauchi, Dai Pra & Sylos Labini 1994), and the Aeolian volcanic activity with magma derived from the subduction zone (Barberi *et al.* 1973). Information about the STSZ regarding the state of stress within the descending slab, at least for its upper part, is lacking.

Since the 1970s the observation of the orientation of *P*- and *T*-axes of earthquake focal solutions has been the most direct way to infer the state of stress within a subduction zone. The distribution of stress axes within subducting slabs has been studied by many authors, including Isacks & Molnar (1971), Vassiliou (1984), Apperson & Frohlich (1987), Vassiliou & Hager (1988) and Zhou (1990). Isacks & Molnar (1971) divided the slabs into two classes based on their depth extension: shallow-extent slabs (<300 km) and deep-extent slabs (>300 km). Shallow-extent slabs are generally characterized by *T*-axes parallel to the slab dip (down-dip tension), whereas deep-extent slabs show down-dip tension above 300 km depth and *P*-axes parallel to the slab dip (down-dip compression)

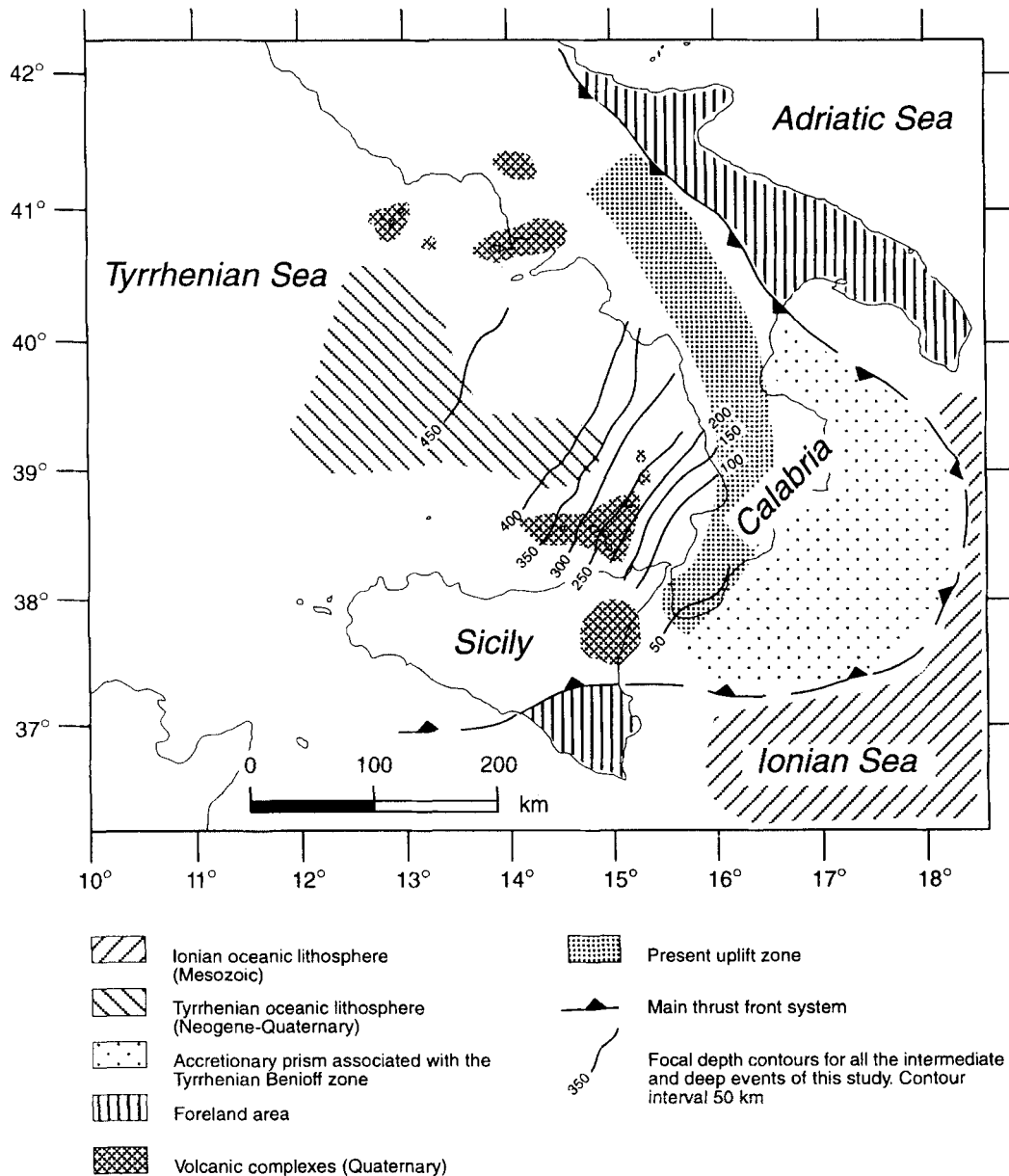


Figure 1. Schematic representation of the main features characterizing the geodynamic active Southern Tyrrhenian region.

below this depth. The deep-extent Tonga slab is a notable exception, showing down-dip P -axes at all depths.

The centroid moment tensor (CMT) solutions reported by the Harvard group (Dziewonski, Chou & Woodhouse 1981) are available for all earthquakes from 1977 onwards with a magnitude m_b greater than 5.2. For studies of stress in the slab prior to 1977 the lower magnitude threshold was generally about $m_b = 5.7$.

From the CMT data, Vassiliou (1984), Vassiliou, Hager & Raefsky (1984) and Apperson & Frohlich (1987) observed that the tendency of P - and T -axes to be aligned with the slab dip is weaker for intermediate earthquakes (70 to 300 km) than for deep events, while the intermediate stress axes (B) are generally clustered along the strike direction at all focal depths. From CMT data for the West Pacific borders' slabs, Zhou (1990) postulated a neutral down-dip zone that divides the

deep down-dip compression from the shallower down-dip tension stress regime within the descending lithosphere.

At present, only CMT solutions of the largest events that occurred in the STSZ and a few other fault-plane solutions are available for the study of the stress distribution within the Tyrrhenian slab (Anderson & Jackson 1987). Since most of these large events occurred in the depth range of 230 to 300 km, information about the stress distribution along the whole slab extension is lacking; therefore, the aim of this study is to improve the knowledge of stress orientation within the STSZ through the analysis of intermediate- and deep-earthquake focal mechanisms. The availability of digital waveforms recorded in the past seven years at numerous seismic stations of the Istituto Nazionale di Geofisica (ING) national seismic network enabled us to compute reliable focal-mechanism solutions for events that occurred in a large portion

of the slab (40 to 450 km) with magnitude >2.7 . In this paper we present new results obtained for 44 well-located events from the past seven years.

GEOMETRY OF THE STSZ

The shape of the slab is important in characterizing the stress distribution within the subducting lithosphere. Since different geometries have been proposed for the STSZ, we review all the available information.

The shape of the subducted lithospheric plate was studied by many authors, using two approaches: seismicity distribution, and tomographic images. The first attempt to delineate the geometry of the STSZ was made by Caputo, Panza & Postpischl (1970) who observed a $\sim 60^\circ$ NNW dipping seismic plane down to 450 km depth beneath the Tyrrhenian Sea using ISC bulletin data. Gasparini *et al.* (1982) and Iannaccone, Scarcella & Scarpa (1985), relocating the ISC and USGS bulletin data with a joint hypocentral determination (JHD) technique, defined a 'spoon-shaped' Benioff zone dipping towards the NW. The zone of maximum concavity was detected between 250 and 340 km depth, corresponding to the highest seismic-energy-release zone.

Anderson & Jackson (1987) revised the intermediate- and deep-earthquake locations reported in the ISC bulletin for the STSZ. They used a rigorous selection of events based on location criteria, defining a planar surface for the Benioff zone dipping to the NW to 500 km depth, approximately 200 km wide along strike. In particular, they inferred a $\sim 70^\circ$ dipping plane from 80 to 250 km, changing to a dip of $\sim 45^\circ$ at depths greater than 250 km. Moreover, Anderson & Jackson (1987) claimed an absence of a 'spoon-shaped' geometry. The anomalous shallowing of the Benioff plane below 250 km depth was also found by Giardini & Velonà (1991), who relocated the ISC bulletin data using a JHD technique. Recently, Selvaggi & Chiarabba (1995) located the earthquakes from the STSZ using both a 1-D and a 3-D velocity model and arrival times at local and regional networks, delineating a continuous slab dipping 70° towards the NW without finding any variation of the Benioff-plane dip in the depth range 100–450 km. They also observed that the events located beneath the Ionian Sea and the Calabrian Arc between 40 and 100 km depth delineate a subhorizontal Benioff plane.

The tomographic image of the Tyrrhenian region, created using teleseismic data recorded at the ING stations (Amato, Cimini & Alessandrini 1990; Amato, Alessandrini & Cimini 1993b), delineate a NW-dipping high-velocity body down to 400–500 km beneath the Southern Tyrrhenian Sea with a velocity contrast of about +5 per cent with respect to the reference model. Other authors (Spakman 1988; Spakman, van der Lee & van der Hilst 1993) computed tomographic images of the entire Mediterranean region using regional arrival times of the ISC bulletins and a 0.8° grid size, obtaining a weak high-velocity anomaly (+2 per cent) for the Tyrrhenian slab. These images show a slab detachment beneath the Calabrian Arc at around 150 km depth (Wortel & Spakman 1992; Spakman *et al.* 1993). An improvement in the spatial resolution of the tomographic images of the STSZ was achieved by Selvaggi & Chiarabba (1995) using regional phases of selected intermediate and deep events from the Tyrrhenian zone. Their results show a continuous NW-dipping, high-velocity body with a large velocity contrast (+5 per cent) and

no clear evidence of slab detachment. We will refer to this geometry in the remainder of the current paper.

PREVIOUS WORK ON THE STRESS DISTRIBUTION WITHIN THE STSZ

Isacks & Molnar (1971) determined both the fault-plane solution for the largest earthquake of the STSZ (1938 April 13, $m_b = 7.1$) and the composite solution of 10 intermediate and deep events (including the 1938 event) that occurred in the period 1938–1962. They found a down-dip P -axis. A more complex situation in the state of stress is delineated by Gasparini *et al.* (1982), who used polarity data from national and international seismological bulletins. They observed two different types of focal-mechanism solutions within the inferred 'spoon-shaped' slab zone, one in the zone of maximum slab concavity with down-dip P -axes and the other with a prevalent strike-slip component for events located both in the northern and southern parts of the slab independent of depth. Anderson & Jackson (1987) observed a down-dip compression stress regime within the subducted Ionian lithosphere from the reliable focal mechanisms of the strongest intermediate and deep earthquakes that occurred in the period 1938–1984. These focal-mechanism solutions mainly covered a depth range from 230 to 300 km. The focal mechanism of the deepest event (1978 December 27, 390 km depth) showed a large strike-slip component. Giardini & Velonà (1991) made a rigorous selection of fault-plane solutions obtained from bulletin data, observing a pervasive down-dip compression for the STSZ.

DATA SELECTION AND ANALYSIS

In this paper, we calculate fault-plane solutions using polarities read at local and regional distances ($\Delta < 500$ km) of earthquakes that occurred after 1988, when the national network of ING increased the coverage of this region. All the waveforms for the Tyrrhenian intermediate and deep earthquakes were repicked to obtain both more accurate arrival times of P and S waves and a larger number of first-motion polarities compared to the routine procedures carried out in the compilation of bulletins. The possible existence of reverse polarities was also investigated through the observation of teleseismic waves of strong, impulsive events.

We have located the intermediate and deep earthquakes using a simple 1-D velocity model (Table 1) and the code Hypoinverse (Klein 1989). We selected the 59 best events (Tables 2 and 3) with a mean of 21 readings. The location errors in the horizontal and vertical directions are, respectively,

Table 1. Velocity model.

Velocity (km s ⁻¹)	Top of layer (km)
5.0	0.0
6.2	10.0
6.7	15.0
8.0	35.0
8.1	100.0
8.2	180.0
8.4	280.0
8.8	400.0

Table 2. Hypocentral parameters, number of stations, magnitude, fault-plane-solution parameters and quality factors for the intermediate and deep events. Latitude and longitude are given in degrees and decimal minutes.

No.	Date	Orig.	Lat. N	Lon. E	Z (km)	ERH	ERZ	No. stat. ¹	m _b ²	M ³	strike	dip	rake	Q _f	Q _p
1	04.08.88	03:57	39 11.07	14 44.71	422	5.1	15.6	24 (29)	4.4	-	20	70	-40	A	A
2	13.11.88	15:19	38 02.13	15 42.30	62	1.4	1.1	14	-	3.1	55	75	-120	A	A
3	15.02.90	04:56	38 43.84	15 05.46	206	2.1	6.8	30 (37)	4.4	-	80	65	-80	A	A
4	18.03.90	22:13	38 59.64	15 32.50	283	3.2	8.2	24	3.5	-	70	70	-80	A	B
5	20.03.90	06:16	39 04.34	15 42.17	162	3.0	6.8	11	-	3.8	0	55	70	A	A
6	25.03.90	18:23	39 12.56	15 14.92	284	3.6	11.5	14	-	3.8	210	5	-150	A	B
7	04.05.90	06:57	38 54.41	15 45.69	106	1.2	3.0	24 (25)	3.5	-	25	65	-60	A	A
8	22.06.90	17:22	38 33.07	15 22.88	174	2.7	7.3	11	3.8	-	40	80	-100	A	B
9	01.08.90	20:33	38 44.22	14 56.68	365	3.1	13.3	11 (14)	4.3	-	345	10	-40	A	B
10	27.08.90	06:51	38 24.69	15 58.99	83	2.3	2.7	15 (18)	-	3.0	55	80	-180	A	B
11	14.12.90	03:21	39 15.09	15 35.02	300	2.2	6.7	36 (41)	5.3	-	95	50	-140	B	A
12	26.02.91	07:25	40 03.06	13 54.45	420	1.8	9.5	48	5.5	-	110	60	160	A	B
13	27.04.91	00:56	38 41.25	15 47.11	94	1.5	2.8	16	-	3.4	145	55	-140	A	A
14	18.05.91	10:08	38 24.29	15 30.03	92	1.5	3.2	12	-	3.2	15	70	-90	A	A
15	06.06.91	01:09	38 18.80	15 31.60	81	2.0	1.8	22	-	3.7	280	90	160	A	A
16	27.08.91	22:03	38 39.05	14 40.90	295	2.6	8.9	20	3.7	-	100	25	-110	B	A
17	27.09.91	13:57	38 56.29	15 40.75	184	4.1	8.2	10	-	3.3	185	35	-70	A	B
18	09.02.92	18:58	39 12.43	15 12.54	324	2.7	5.0	20	3.5	-	120	40	-120	B	A
19	12.03.92	07:22	38 25.72	15 16.56	154	2.0	3.3	16 (17)	-	3.7	20	20	-40	A	A
20	25.04.92	12:46	38 34.17	14 54.80	225	1.5	6.1	54	5.4	-	355	30	-20	B	A
21	26.04.92	23:28	38 37.67	14 45.30	259	2.2	11.7	11	-	3.8	165	10	-140	B	A
22	22.05.92	18:49	39 49.53	15 09.08	432	4.8	15.4	12	3.8	-	135	25	110	B	A
23	25.06.92	21:27	38 39.06	15 04.74	251	2.0	3.6	29 (40)	4.1	-	35	70	-100	B	B
24	03.07.92	22:03	37 45.52	15 53.74	48	1.8	2.2	15	-	3.1	145	50	-90	A	A
25	10.07.92	04:24	38 52.67	15 40.10	163	2.9	5.5	9	-	3.2	120	45	20	A	A
26	04.08.92	21:54	39 26.64	15 33.15	262	1.7	4.1	28	4.3	-	120	40	-160	B	A
27	23.09.92	14:41	38 14.66	15 32.93	136	2.6	3.0	13	-	3.4	60	30	70	A	B
28	28.10.92	16:25	38 00.45	15 47.40	54	1.5	1.6	12 (14)	-	3.4	220	80	120	A	A
29	29.10.92	16:49	38 40.76	15 22.18	146	4.0	3.7	9	-	3.1	110	75	70	A	B
30	26.12.92	06:46	38 25.64	15 27.92	95	2.3	6.9	11	-	2.9	0	55	90	A	A
31	22.03.93	23:44	38 11.38	15 45.40	78	1.6	1.7	10 (13)	-	2.7	110	55	-160	A	A
32	08.08.93	13:57	38 41.05	15 35.21	168	3.3	4.7	13	-	3.2	110	30	-60	A	A
33	31.08.93	00:16	39 56.73	15 15.81	335	2.0	7.0	49	4.7	-	75	75	-150	B	A
34	17.09.93	20:00	38 50.05	15 52.81	199	2.9	6.5	18 (20)	-	3.6	295	90	90	A	B
35	17.09.93	22:34	38 23.97	15 26.88	137	4.4	5.9	19	-	3.1	0	90	-30	A	A
36	31.10.93	03:49	38 58.76	15 23.74	278	1.5	2.1	26 (31)	-	3.9	190	30	-100	B	A
37	27.11.93	13:26	38 47.83	14 57.17	300	2.0	4.6	53	4.8	-	60	60	-90	A	B
38	05.01.94	13:24	39 00.48	15 23.85	298	2.5	8.4	36	5.7	-	60	60	-80	A	B
39	06.01.94	12:28	39 37.10	15 37.74	326	2.5	7.7	28	4.1	-	45	40	-150	A	A
40	21.03.94	21:41	39 40.18	15 41.04	287	2.0	4.4	39	5.1	-	155	5	-150	A	A
41	25.04.94	23:51	38 39.28	15 27.66	155	2.0	4.3	20	-	3.6	335	65	30	A	A
42	03.05.94	08:27	39 04.12	15 03.92	338	4.1	14.3	18	3.7	-	120	60	-120	A	A
43	22.05.94	11:23	38 39.77	15 28.71	133	3.0	6.4	12	-	3.2	55	85	-20	A	A
44	12.06.94	03:26	38 38.14	15 24.98	147	3.3	3.8	10	-	3.4	40	70	140	A	A

1 Number of stations with polarity and in brackets stations utilized for location.

2 Magnitude from NEIC.

3 Magnitude from ING.

ERH and ERZ are the horizontal and vertical location uncertainties (km), respectively.

Q_f and Q_p are the fault plane solution quality factors (see TABLE 4).

Table 3. Hypocentral parameters, number of stations and magnitude for the intermediate and deep events with fault-plane solutions rejected. Latitude and longitude are given in degrees and decimal minutes.

No.	Date	Orig.	Lat.N	Lon.E	Z (km)	ERH	ERZ	No. stat.	M ¹
1	06.04.89	03:30	38 32.19	15 22.65	143	3.5	6.9	7	2.8
2	24.06.90	23:02	38 13.10	15 02.11	154	2.8	4.1	10	3.7
3	21.08.91	02:41	39 04.12	16 05.79	83	1.4	3.2	14	3.8
4	05.02.92	22:39	39 19.69	14 46.30	401	6.4	10.8	13	3.9
5	24.02.92	16:13	37 37.77	16 35.55	52	15.1	20.2	8	2.9
6	06.08.92	23:45	38 28.20	15 34.12	67	1.6	6.4	7	3.0
7	29.11.92	03:22	37 35.32	15 12.07	80	3.3	3.9	10	3.2
8	20.03.93	01:18	38 08.84	16 32.90	43	2.7	3.9	15	3.4
9	16.07.93	15:06	38 42.75	14 42.49	284	3.2	5.6	21	3.8
10	26.07.93	22:01	38 17.33	14 34.11	145	2.0	5.7	13	2.8
11	21.01.94	19:34	39 19.80	15 40.89	272	3.4	9.3	17	4.2
12	16.03.94	14:49	38 17.16	14 37.26	179	1.6	4.7	18	3.6
13	24.06.94	04:34	38 36.19	15 35.06	84	1.8	3.8	11	2.9
14	23.08.94	20:30	38 34.90	14 57.75	223	1.8	5.0	22	3.7
15	11.09.94	01:44	39 29.00	15 30.41	263	2.3	5.6	17	3.9

1 Magnitude from ING.

3 and 6 km on average. The hypocentral depths range between 40 and 440 km.

The map view of Fig. 2(a) shows the distribution of the 59 selected events, whose epicentres are mainly concentrated offshore of the Calabrian Arc. The NW–SE section, A–A' in Fig. 2(b), shows that the seismicity is almost continuous from 40 to 350 km, with two different slab dips. Between 40 and 70–80 km depth the slab is subhorizontal (Fig. 2b); below this depth it bends, and from 100–120 km down to 350 km it has a constant dip of $\sim 70^\circ$. This geometry is in agreement with that found by Selvaggi & Chiarabba (1995), who analysed a more complete data set covering the same period (Figs 3a and b). Below 350 km depth the hypocentres are spread over a large zone.

Using the Selvaggi & Chiarabba (1995) data set, we try to characterize the lateral variation of the slab geometry with three parallel NW–SE sections, as shown in Fig. 3(a). The upper portion of the Benioff zone (40–180 km depth) is well defined in the southern-most section (A–B, Fig. 3c). The section C–D (Fig. 3d) in the middle part of the STSZ is characterized by a rather continuous seismicity ranging from 40 to 330 km depth with a well-delineated Benioff plane dipping 70° NW. Widespread seismicity occurs in the northernmost section (E–F, Fig. 3e). Here we observe the deepest part of the Benioff zone and a seismic gap between 120 and 200 km. It is possible that this spatial gap is due to the short period of observations (7 yr).

The fault-plane solutions were determined using the program FPFIT (Reasenber & Oppenheimer 1985). Focal mechanisms are ranked examining their quality factors: the first (Q_f) reflects the solution prediction misfit to the polarity data, F_j ($F_j = 0.0$ is a perfect fit to the data, while $F_j = 1.0$ is a perfect misfit), and the second (Q_p) reflects the solution uniqueness, in terms of the 90 per cent confidence region, on strike, dip and rake. Following Hartse *et al.* (1994), we assigned three classes for

Table 4. Fault-plane-solution quality factors Q_f and Q_p . F_j is the solution prediction misfit to the polarity data. Δ_s , Δ_d and Δ_r are ranges of perturbations to the strike, dip and rake, respectively (see text).

Q_f		Q_p	
A	$F_j \leq 0.025$	A	$\Delta_s, \Delta_d, \Delta_r \leq 20^\circ$
B	$0.025 < F_j \leq 0.1$	B	20° to 40°
C	$F_j > 0.1$	C	$> 40^\circ$

each quality factor (A, B and C; see Table 4). 22 focal mechanisms have quality A–A (Q_f – Q_p), 21 have quality A–B or B–A, while only one has quality B–B. The 15 focal mechanisms with quality C for one of the two quality factors were rejected; our final data set therefore consists of 44 well-constrained fault-plane solutions.

STATE OF STRESS WITHIN THE STSZ

The 44 focal mechanisms (Fig. 4) are divided into three sets according to different depth ranges (40–165 km, 165–370 km and 370–450 km) (Figs 5a, b and c). We choose these subdivisions by considering the relative homogeneity in the P -axis distributions within each class.

In the upper depth interval (40–165 km; Fig. 5a) we find both normal, reverse and strike-slip solutions. Observing the epicentral distribution, there are two main epicentral regions: one located NW of the Messina Strait, with six events ranging from 81 to 154 km depth, and the second located SE of Stromboli Island, with four events ranging from 133 to 155 km depth. The other epicentres are scattered partly in the Tyrrhenian Sea and partly in the southern portion of the

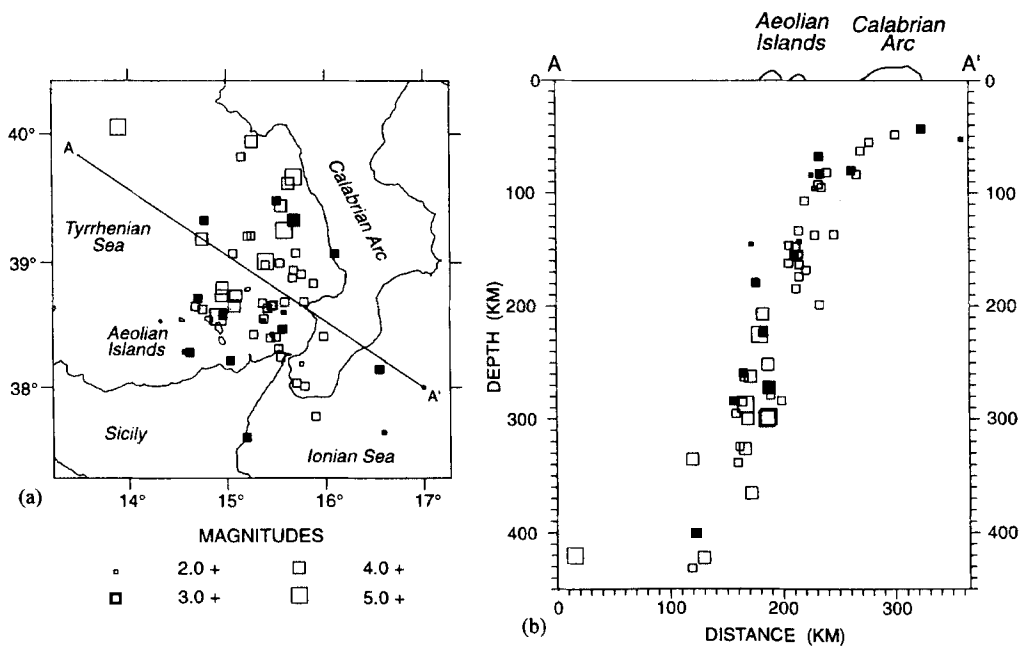


Figure 2. (a) Epicentral distribution of the 59 selected intermediate and deep events of the period 1988–1994 of the Southern Tyrrhenian Sea. Magnitudes are indicated by squares of different sizes. Filled squares indicate the epicentres of the 15 events with focal mechanisms rejected. (b) NW–SE section through the Southern Tyrrhenian Sea and the Calabrian Arc.

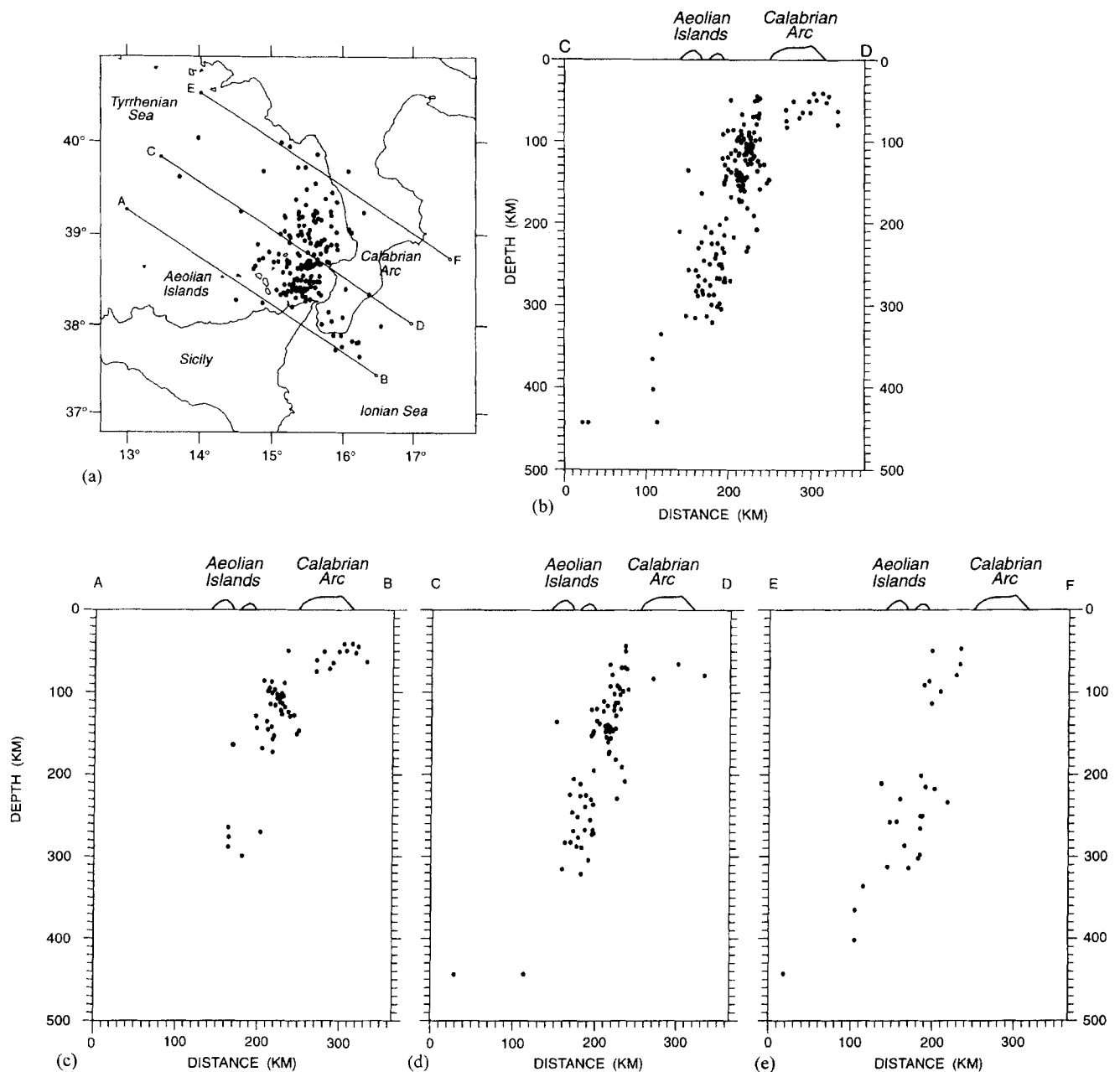


Figure 3. (a) Epicentral distribution of 185 Southern Tyrrhenian earthquakes selected from Selvaggi & Chiarabba (1995) for the period 1988–1994. (b) NW–SE section across the Southern Tyrrhenian subduction zone with all event hypocentres. (c), (d), (e) NW–SE sections (see map).

Calabrian peninsula, characterized by shallow hypocentres (depth, z , < 100 km). The focal solutions of three of these latter events (48, 62 and 78 km depth) have a prevalent normal component. Of the other two mechanisms, one has a prevalent reverse component (54 km depth) and one has an almost pure strike-slip solution (83 km depth). The strike-slip component is also prevalent for the 81 and 137 km depth solutions belonging to the epicentral cluster located NW of the Messina Strait and the 133 km depth solution of the epicentral cluster located SE of Stromboli Island. The focal-mechanism solutions of the events located NW of the Messina Strait show normal, reverse and strike-slip solutions for earthquakes located close to each other, reflecting the heterogeneity of the 40–165 km depth range. In the depth interval of 146 to 165 km the focal

mechanisms show a prevalence of reverse solutions, with the exception of one normal event (154 km depth). The epicentres of those events with reverse solutions are partly concentrated SE of Stromboli Island and partly W of the St. Eufemia Gulf.

In the 165–370 km depth range (Fig. 5b) the epicentres are shifted to the NW with respect to the previous interval, following the dip of the Benioff plane. The epicentres are scattered in an area ranging from the Aeolian Islands, the St. Eufemia Gulf and the Policastro Gulf. This epicentral distribution does not show any evident cluster. Fault-plane solutions with a prevalent normal component (nearly vertical P -axes) characterize this depth interval.

In the deepest depth range, from 370 to 450 km (Fig. 5c),

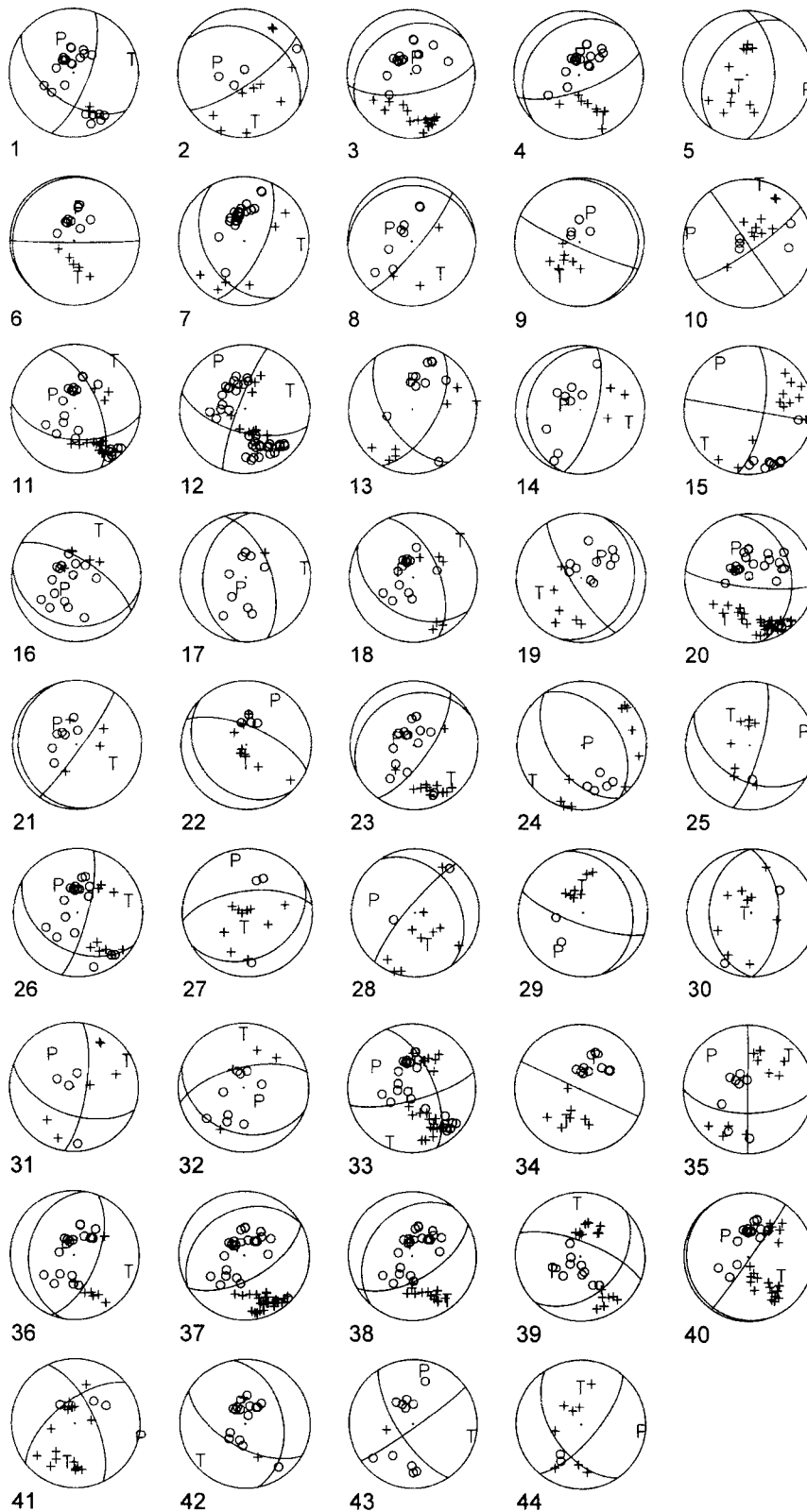


Figure 4. Fault-plane solutions with first-motion polarities for the 44 selected intermediate and deep events of the Tyrrhenian subduction zone.

we computed focal mechanisms for only three events, with hypocentres concentrated between 420 and 432 km depth. The solution with a prevalent strike-slip component belongs to the event closer to the central part of the Tyrrhenian Sea. The

other two events, one located north of the Aeolian Islands at 422 km depth and one located off-shore of the southern Campania coast at 432 km depth, have solutions with prevalent normal and prevalent reverse components, respectively.

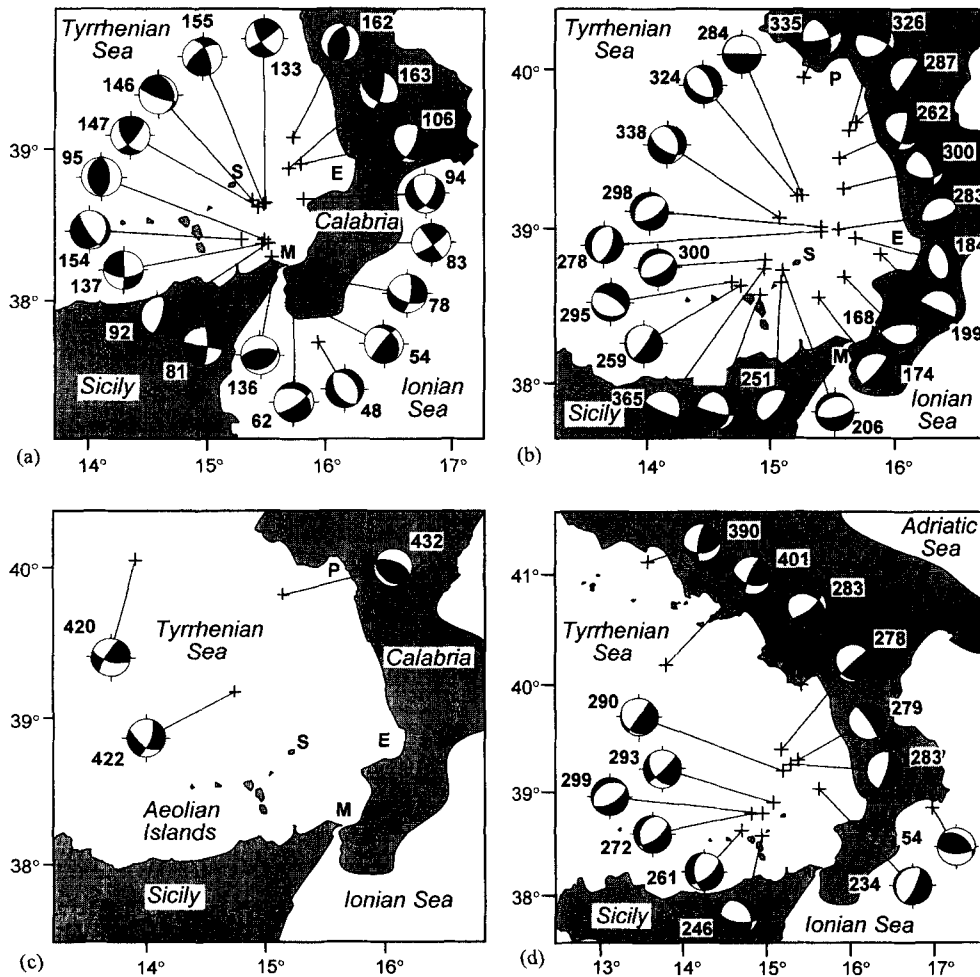


Figure 5. Focal mechanisms of the intermediate and deep Tyrrhenian events of this study (Table 2) subdivided into three depth intervals: (a) 40–165 km; (b) 165–370 km; (c) 370–450 km. M, S, E and P indicate the Messina Strait, Stromboli Island, the St. Eufemia Gulf and the Policastro Gulf, respectively. (d) Focal mechanisms of the strongest intermediate and deep earthquakes of the Tyrrhenian Sea of the period 1938–1994 with magnitude $m_b \geq 4.8$ (Table 5). The hypocentral depth is indicated next to each solution in km.

To compare the seismic release in the period analysed in this study (1988–1994) with the long-term behaviour of the slab, we considered the largest earthquakes to have occurred in the STSZ after instrumental data became available. Fig. 5(d) shows the fault-plane solutions of the largest ($m_b > 4.8$) inter-

mediate and deep earthquakes that occurred in the period 1938–1994 reported by Anderson & Jackson (1987) and in the CMT catalogue (Table 5). All the events included in the 230–300 depth range have normal focal mechanisms. The two deepest events (390 and 401 km depth) show a large strike-slip

Table 5. Hypocentral parameters and magnitudes for the strongest intermediate and deep events of the period 1938–1994. The m_b values of the first three earthquakes are from Karnik (1969) and Rothè (1969).

No.	Date	Lat.N	Lon.E	z (km)	m_b	Source
1	13.04.38	39 12.00	15 12.00	290	7.1 (m _B)	Anderson and Jackson 1987
2	01.02.56	39 01.80	15 37.80	234	6.2 (m _B)	"
3	03.01.60	39 15.60	15 17.40	283	6.2 (m _B)	"
4	20.12.73	38 47.64	14 49.32	272	4.9	"
5	28.06.77	38 37.80	14 42.72	261	5.0	"
6	15.08.77	38 51.00	16 58.80	54	5.0	CMT catalogue
7	30.12.77	40 00.00	15 25.14	283	5.4	"
8	27.12.78	41 06.48	13 34.92	390	5.4	"
9	21.03.84	39 25.14	15 14.04	278	5.1	"
10	14.12.90	39 18.00	15 22.80	279	5.3	"
11	26.02.91	40 10.80	13 48.00	401	5.5	"
12	25.04.92	38 34.80	14 57.00	246	5.4	"
13	27.11.93	38 47.83	14 57.17	299	4.8	"
14	05.01.94	38 54.00	15 05.00	293	5.7	"

component and the only intermediate-depth earthquake (54 km) beneath the Ionian coast of Calabria has a reverse mechanism. Most of the large earthquakes that occurred in this period (11 out of 14) are concentrated in the depth range 230–300 km.

The directions of *P*- and *T*-axes of the 44 events, covering approximately the whole slab, improve the information achieved using only the solutions from the strongest earthquakes of the period 1938–1994. Figs 6 and 7 show the *P*- and *T*-axis distributions of our data in comparison with the CMT solutions for the strongest events. Our data permit three different intervals of the slab to be recognized, characterized by different distributions of *P*- and *T*-axes.

Between 165 km and 370 km depth (where the slab is continuously dipping 70° towards the NW), the *P*-axes are concentrated in the NW quadrant and their average dip is around 66°, indicating down-dip compression, similar to what has been found for the CMT solutions. The average dip has been estimated by simple Bingham statistics (Onstott 1980), providing a 95 per cent confidence region of 10.2°.

It is interesting to observe the similar distribution of *P*-axes between the two data sets in this depth interval. The *T*- (or *B*-) axes are perpendicular (or parallel) to the slab direction only for the largest earthquakes (CMT solutions), while the *T*-axes

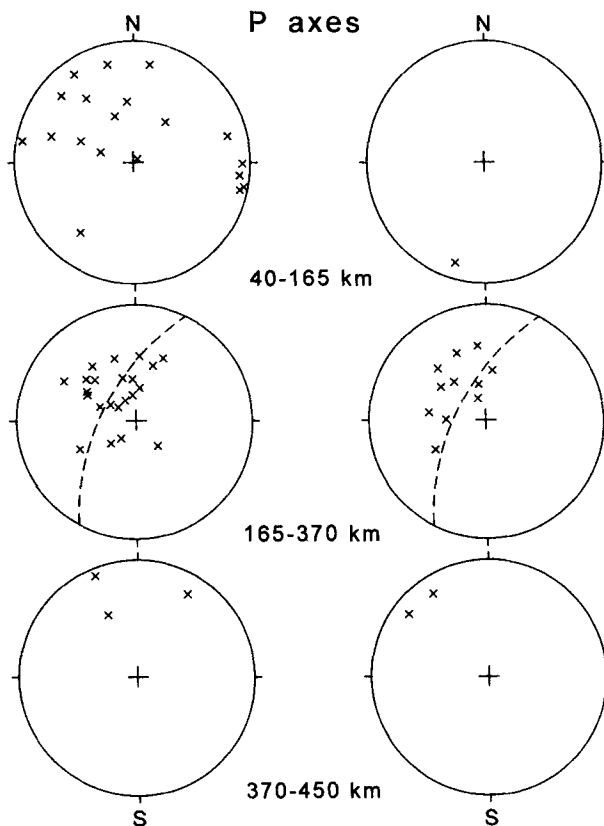


Figure 6. *P*-axis distribution of the solutions determined in this study (on the left) and those of the strongest events of the period 1938–1994 (on the right) (from Anderson & Jackson 1987 and the CMT catalogue). The *P*-axes are plotted on a stereographic projection. The depth ranges are the same as in Fig. 5. The dashed line on the plot of the 165–370 km depth interval is the projection of the Benioff plane dipping 70°.

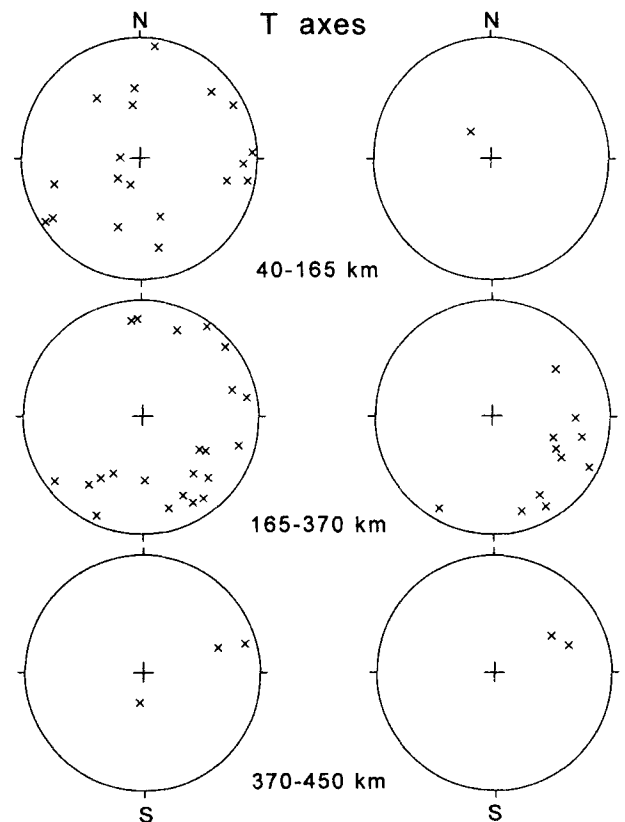


Figure 7. *T*-axis distribution of the solutions determined in this study (on the left) and those of the strongest events of the period 1938–1994 (on the right) (from Anderson & Jackson 1987 and the CMT catalogue). The *T*-axes are plotted on a stereographic projection. The depth ranges are the same as in Fig. 5.

are either orthogonal or parallel to the slab's strike for smaller magnitude events (Fig. 7).

At greater depths (370–450 km), we observe subhorizontal *P*-axes, both for the three events of our data set, and for the two CMT solutions, which are distributed in the NW and NE quadrants (Figs 6 and 7). Few strong earthquakes occur in this interval and the tomographic velocity images are less clear in this deep part of the slab (Amato *et al.* 1993a).

SEISMIC ENERGY RELEASE AT DEPTH

Anderson & Jackson (1987) observed a pronounced concentration of energy release at depths of 230–300 km, although they remarked that there are no significant gaps in the seismicity distribution along the entire slab length. They also warned that their analysis was based on a 20 yr period (with the addition of three earlier events of the period 1938–1960), of only moderate [$4.5 < \text{magnitude } (M) < 6.5$] and strong ($M > 6.5$) events. In our study, based only on 7 yr of observation, we have also found that a higher seismic activity is concentrated in approximately the same depth interval, as shown in Fig. 2(b). The map view of Fig. 2(a) shows that the strongest earthquakes are concentrated in an extended and quite narrow zone, trending NE from the Aeolian Islands to the northern Calabrian coast (around latitude 40°N). This confirms that this deep portion of the slab is indeed the part where the highest energy release occurs. The most intense

activity of our data set is concentrated between ~ 190 and 370 km depth, a greater interval than that suggested by Anderson & Jackson (1987) (230–300 km).

The histogram in Fig. 8(a) shows the seismic-energy distribution with depth, considering only the events of our data set (1988–1994). Only four seismic moments for the strongest earthquakes are available from the NEIC bulletins. The others are determined from the equation $\log M_0 = (m_b + 2.6)/0.45$, obtained by the regression of magnitudes m_b against the CMT seismic moments for significant earthquakes of the Mediterranean region since 1977 (Giardini, Palombo & Boschi 1993). The bars show the distribution of cumulative seismic moments at each 30 km depth interval. We observe a moderate

release of seismic energy between 190 and 370 km depth with seismic moments over 2.1×10^{15} N m. Smaller events with seismic moments ranging from 3.6×10^{13} to 4.3×10^{14} N m are concentrated in the upper slab portion (40–190 km). The deepest slab portion (400–460 km), characterized by few events, also shows a moderate release of seismic energy (up to 1.1×10^{17} N m for M_0).

Fig. 8(b) shows the seismic energy distribution when only the moderate and high intermediate and deep seismicity ($m_b > 4.9$) of the period 1938–1987 is considered (see Table 5). Note the concentration of energy in the 220–310 km depth interval, with M_0 ranging from 5.3×10^{17} to 5.7×10^{19} N m. Two isolated large events are present in this period, at 54 and

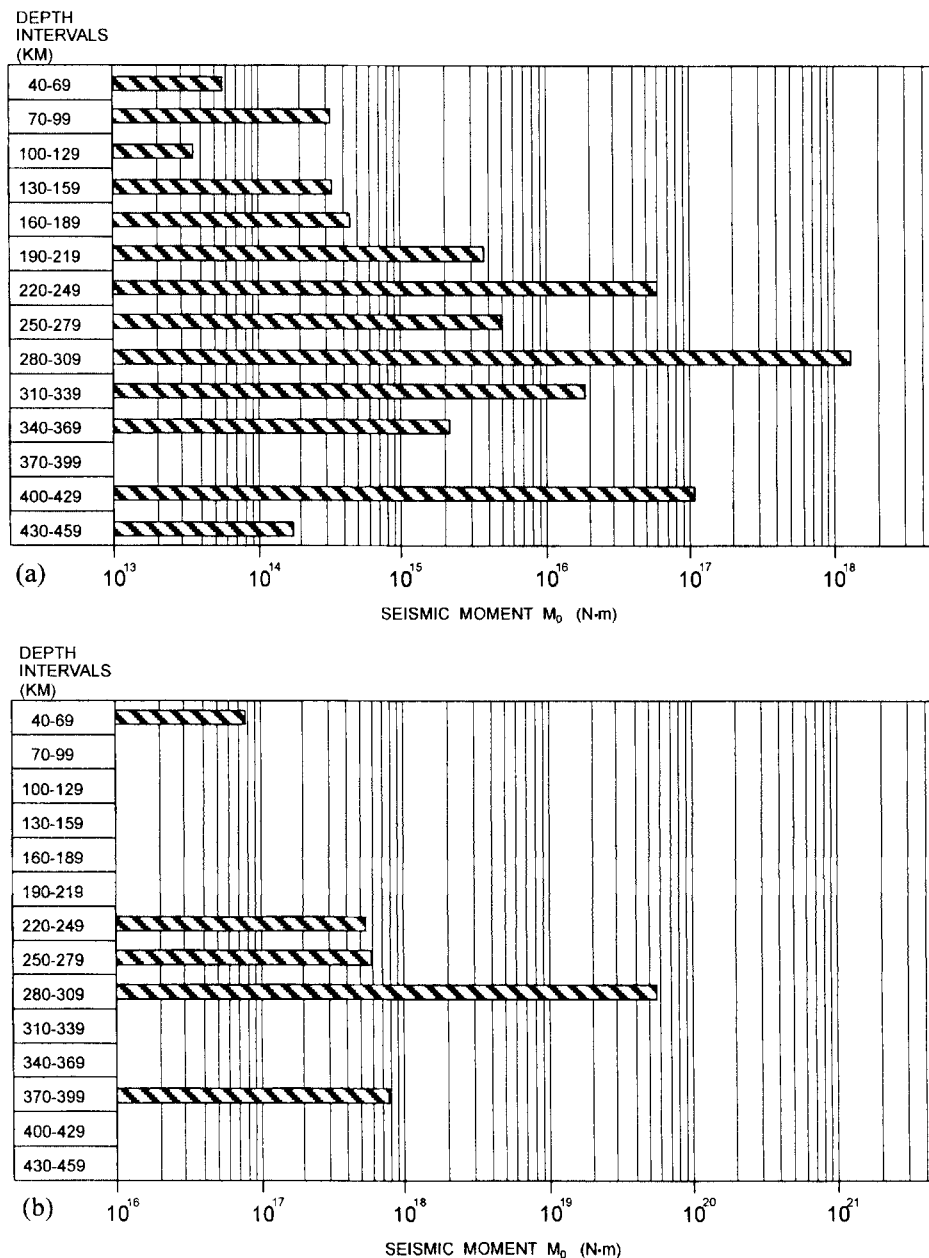


Figure 8. Histograms on a logarithmic scale showing the depth distribution of cumulative seismic moments. On the ordinate axis depth is divided into intervals of 30 km. (a) Seismic moments of the 59 events of this study (1988–1994), (b) seismic moments of the strongest events of the period 1938–1987. The seismic moment of the first three events of Table 5 with m_b values are calculated through the regression of m_b versus M_w (Kanamori 1983) and with the equation $\log M_0 = 1.5 M_w + 16.1$ (Kanamori 1977).

390 km depth with seismic moments of 7.7×10^{16} and 7.7×10^{17} N m, respectively.

Our data quantify the seismic energy in the shallow part of the slab. The upper portion of the STSZ (40–190 km) is characterized by a lower level of seismicity compared with the intermediate portion (190–370 km). At greater depths (400–460 km) seismic energy is moderate, with cumulative seismic moments ranging from 1.7×10^{14} to 1.1×10^{17} N m. In this depth range the seismic energy is released by a few large events. It is interesting to note the correspondence between the depth interval with the highest level of seismicity and that in which *P*-axes are close to the slab dip (165–370 km).

DISCUSSION

The location of intermediate and deep earthquakes recorded since 1988 at the ING national seismic network shows the existence of a continuous distribution of seismicity from 40 to 370 km depth (see also Selvaggi & Chiarabba 1995). At greater depths the seismicity is sporadic and widespread in a large zone, characterized by large earthquakes. In the slab's upper portion (40–100 km depth) the subducted Ionian lithosphere is subhorizontal (Fig. 2b). Below 100 km the slab bends and the dip increases to about 70°. The shallowing of the slab dip from 70° to 45° at 250 km depth suggested by previous investigators (Anderson & Jackson 1987; Giardini & Velonà 1991) is not observed. The slab's shallower portion (40–100 km depth) is more evident in the SW part of the subduction zone (i.e., between north-eastern Sicily and the southern tip of Calabria, Fig. 3c), whereas the intermediate and deeper parts are well delineated in the middle and northern part (central and northern Calabria, respectively; Figs 3d and e). The 44 well-constrained focal mechanisms determined in this study, relative to the best-located events of the past 7 yr, allow us to gain information about the deformation in a large portion of the southern Tyrrhenian slab. The slab can be divided into three parts from the distribution of *P*-axes (Fig. 6). In the upper part of the slab (40–165 km), which includes both the subhorizontal part of the slab and the bending portion, the fault-plane solutions are strongly heterogeneous. Normal, reverse and strike-slip solutions are present. In particular, we note the presence, with only one exception, of reverse fault-plane solutions in the 146–165 km depth interval. However, *P*-axes in the shallow portion of the slab tend to concentrate in the NW quadrant. In this depth interval only a few data were analysed in previous works (Gasparini *et al.* 1982; Iannaccone *et al.* 1985). In the intermediate portion of the slab, ranging from 165 to 370 km depth, the fault-plane solutions are more homogeneous. This depth interval is characterized by a consistent direction of down-dip compression (*P*-) axes. The deepest portion of slab (370–450 km) shows three focal mechanisms with a prevalent strike-slip component.

For the entire slab length the *P*-axes mostly plunge towards the NW, coinciding with the dip direction of the slab. Mechanisms for earthquakes occurring in the intermediate portion of the slab (200–300 km) most clearly indicate down-dip compression, in agreement with previous studies (Isacks & Molnar 1971; Gasparini *et al.* 1982; Iannaccone *et al.* 1985; Anderson & Jackson 1987; Giardini & Velonà 1991).

The analysis of a larger number of events, though of small magnitudes, allows us to infer that the slab is characterized by diffuse down-dip compression in a greater depth interval

(165–370 km) than has been observed in previous studies that considered only stronger earthquakes. Such a diffuse down-dip compression along almost the entire slab extension is anomalous, since in most deep slabs the down-dip compression is evident only at depths exceeding 300 km (Isacks & Molnar 1971; Vassiliou 1984).

The depth distribution of seismic energy within the continuous southern Tyrrhenian slab is characterized by a low level of seismicity between 40 and 190 km depth, whereas in the 190–370 km depth interval the cumulative seismic moments for each 30 km depth interval range between 2.1×10^{15} and 6.2×10^{19} N m (Fig. 8). The deepest slab portion (370–450 km) shows moderate seismic energy released by few events.

Through both a long observation period of strong earthquakes (1938–1987) and a shorter period (1988–1994) of lower-magnitude events (see Fig. 8), we conclude that most of the southern Tyrrhenian slab's seismic activity is concentrated in the 190–370 km depth interval. Note the good correspondence between the high-seismic-energy depth interval and that characterized by a clear down-dip distribution of *P*-axes.

In comparison with other subduction zones, the STSZ is anomalous both in seismicity and in down-dip compression/tension distribution with depth. Two types of slab have been proposed by Isacks & Molnar (1971) and Vassiliou & Hager (1988) based on their length: shallow-extent slabs, with maximum depth above 300 km, and deep slabs, extending to 670 km depth. The STSZ, with its continuous seismicity up to 350 km and the small and scattered deep seismicity down to about 450 km, is intermediate between these two types. Also, the width of the STSZ (only 200 km in a NE–SW direction) is anomalously small in comparison to its depth dimension.

Many authors have claimed that the STSZ is driven solely by the slab-pull force of a passively sinking slab (Patacca & Scandone 1989; Royden 1993; Bassi & Sabadini 1994). According to this hypothesis, the upper portion of the slab should generally be characterized by down-dip tension, whereas a down-dip compression is predicted below about 300 km depth (Isacks & Molnar 1971; Vassiliou 1984). On the contrary, we note that the STSZ slab is characterized by down-dip compression below 165 km and by a complicated and heterogeneous distribution of *P*- and *T*-axes from 40 to 165 km. We have no indication of down-dip tension within the STSZ slab (see Fig. 7).

Giunchi *et al.* (1995) modelled the stress distribution at depth for the STSZ, constraining the slab geometry with tomographic reconstructions. The driving mechanism in their model is slab pull, which reproduces many features of the STSZ well, including the morphology of the trench-forearc region. However, if the stress field is being generated solely by slab pull, a prevalent down-dip tension is predicted along the slab down to 300 km. Trying to reproduce the observed stress pattern, Giunchi *et al.* (1995) introduced an increase of viscosity below the transition zone at 400 km depth. In the resulting stress pattern within the subducting slab, a down-dip compression at depths between 160 and 350 km is predicted in the top of the slab, whereas extension between 160–350 km in the inner part of the slab is strongly reduced (Giunchi *et al.* 1995). This model fits our data better, although the present data set does not allow us to infer details of the stress distribution within the slab or in its upper layer. Nevertheless, the predicted style of faulting in the shallower portion of the slab is still dominated by extension, both in the upper- and in

the inner-slab layers. Conversely, we observe that most *P*-axes are oriented along the slab dip (Fig. 6). This suggests that other mechanisms besides pure slab pull play a significant role in the Tyrrhenian subduction process. The observed internal deformation of the slab (down-dip compression) can be related to the penetration of the slab into a high-strength mantle.

CONCLUSION

The STSZ is characterized by continuous seismicity from 40 to 370 km depth. Beneath 370 km the seismicity is episodic and scattered in a large volume, reaching approximately 450 km depth. Beneath the Ionian Sea and the Calabrian Arc, between 40 and 100 km depth, the Benioff plane is subhorizontal. Below this depth interval it dips 70° to the NW. We do not observe a 'spoon-shaped' Benioff zone, nor a change in slab dip around 250 km depth. From the 59 selected events (*M* 2.7–5.7) that occurred between 1988 and 1994, we determined 44 focal-mechanism solutions. In the 40–165 km depth interval, normal, reverse and strike-slip solutions are observed, with *P*-axes generally oriented in the direction of the slab but with different dips. For events in the depth interval 165–370 km, the focal-mechanism solutions all exhibit a prevalent normal component and are decidedly down-dip. The mechanisms of earthquakes in the deepest interval (370–450 km) exhibit *P*-axes that have a shallow dip. The seismic-energy release of the slab during the past 50 yr is similar to that observed during the last 7 yr. The depth interval of highest seismic-energy release corresponds to the interval characterized by down-dip compression. The distribution of compressional axes is inconsistent with model predictions for a purely sinking slab. Rheological heterogeneities and an active convergence between the African and Eurasian plates may account for the observed diffuse down-dip compression.

ACKNOWLEDGMENTS

We are grateful to two anonymous referees for reviewing this paper and to Franco Missori for his kindness in providing us with the digital data.

REFERENCES

Amato, A., Cimini, G.B. & Alessandrini, B., 1990. Teleseismic residuals and *P*-velocity distribution in Italy from the analysis of digital waveforms, *Proc. XXII General Assembly ESC*, Barcelona, 77 (abstract).

Amato, A., Alessandrini, B., Cimini, G.B., Frepoli, A. & Selvaggi, G., 1993a. Active and remnant subducted slabs beneath Italy: evidence from seismic tomography and seismicity, *Ann. Geofis.*, **36**, 201–214.

Amato, A., Alessandrini, B. & Cimini, G.B., 1993b. Teleseismic wave tomography of Italy, in *Seismic Tomography: Theory and practice*, pp. 361–397, eds Iyer, H.M. & Hirahara, K., Chapman and Hall, London.

Anderson, H. & Jackson, J., 1987. The deep seismicity of the Tyrrhenian Sea, *Geophys. J. R. astr. Soc.*, **91**, 613–637.

Apperson, K.D. & Frohlich, C., 1987. The relationship between Wadati–Benioff zone geometry and *P*, *T* and *B* axes of intermediate and deep focus earthquakes, *J. geophys. Res.*, **92**, 13 821–13 831.

Barberi, F., Gasparini, P., Innocenti, F. & Villari, L., 1973. Volcanism of the southern Tyrrhenian Sea and its geodynamic implications, *J. geophys. Res.*, **78**, 5221–5232.

Barberi, F. et al., 1978. Age and nature of basalts from the Tyrrhenian abyssal plain, *Init. Rep. Deep Sea drill. Proj.*, **42**, 509–514.

Bassi, G. & Sabadini, R., 1994. The importance of subduction for the modern stress field in the Tyrrhenian area, *Geophys. Res. Lett.*, **21**, 329–332.

Caputo, M., Panza, G.F. & Postpischl, D., 1970. Deep structure of the Mediterranean Basin, *J. geophys. Res.*, **75**, 4919–4923.

Dercourt, J. et al. 1986. Geological evolution of the Tethys belt from the Atlantic to the Pamirs since the Lias, *Tectonophysics*, **123**, 241–315.

Dewey, J.F., Pitman, W.C., Ryan, W.B.F. & Bonin, J., 1973. Plate tectonics and the evolution of the Alpine system, *Bull. geol. Soc. Am.*, **84**, 3137–3184.

Dogliani, C., 1991. A proposal for the kinematic modelling of W-dipping subductions—possible applications to the Tyrrhenian–Apennines system, *Terra Nova*, **3**, 423–434.

Dziewonski, A.M., Chou, T.A. & Woodhouse, J.H., 1981. Determination of earthquake source parameters from waveform data for studies of global and regional seismicity, *J. geophys. Res.*, **86**, 2825–2852.

Gasparini, C., Iannaccone, G., Scandone, P. & Scarpa, R., 1982. Seismotectonics of the Calabrian Arc, *Tectonophysics*, **84**, 267–286.

Giardini, D. & Velonà, M., 1991. The deep seismicity of the Tyrrhenian Sea, *Terra Nova*, **3**, 57–64.

Giardini, D., Palombo, B. & Boschi, E., 1993. The determination of earthquake size and source geometry in the Mediterranean Sea, in *Recent Evolution and Seismicity of the Mediterranean Region*, pp. 213–238, eds Boschi, E., Mantovani, E. & Morelli, A., Kluwer, Dordrecht.

Giunchi, C., Sabadini, R., Boschi, E. & Gasparini, P., 1995. Dynamic models of subduction: geophysical and geological evidence in the Tyrrhenian, *Geophys. J. Int.*, accepted.

Hartse, H.E., Fehler, M.C., Aster, R.C., Scott, J.S. & Vernon, F.L., 1994. Small-scale stress heterogeneity in the Anza seismic gap, Southern California, *J. geophys. Res.*, **99**, 6801–6818.

Hutchison, I., von Herzen, R.P., Loudon, K.E., Sclater, J.G. & Jemsek, J., 1983. Heat flow in the Balearic and Tyrrhenian Basins, western Mediterranean, *J. geophys. Res.*, **90**, 685–701.

Iannaccone, G., Scarcella, G. & Scarpa, R., 1985. Subduction zone geometry and stress patterns in the Tyrrhenian Sea, *Pageoph*, **123**, 819–836.

Isacks, B. & Molnar, P., 1971. Distribution of stresses in the descending lithosphere from a global survey of focal-mechanism solutions of mantle earthquakes, *Rev. Geophys. Space Phys.*, **9**, 103–174.

Kanamori, H., 1977. The energy release in greatest earthquakes, *J. geophys. Res.*, **82**, 2981–2987.

Kanamori, H., 1983. Magnitude scale and quantification of earthquakes, *Tectonophysics*, **93**, 185–199.

Karnik, V., 1969. *Seismicity of the European Area*, Reidel, Dordrecht.

Klein, F.W., 1989. Hypoinverse, a program for Vax computers to solve for earthquake location and magnitude, *USGS Open file rept*, no. 89-314.

Malinverno, A. & Ryan, W.B.F., 1986. Extension in the Tyrrhenian Sea and shortening in the Apennines as result of arc migration driven by sinking of the lithosphere, *Tectonics*, **5**, 227–245.

Miyauchi, T., Dai Pra, G. & Sylos Labini, S., 1994. Geochronology of Pleistocene marine terraces and regional tectonics in the Tyrrhenian coast of South Calabria, Italy, *Il Quatern.*, **7**, 17–34.

Onstott, T.C., 1980. Application of the Bingham distribution function in paleomagnetic studies, *J. geophys. Res.*, **85**, 1500–1510.

Patacca, E. & Scandone, P., 1989. Post-Tortonian mountain building in the Apennines. The role of the passive sinking of a relic lithospheric slab, in *The Lithosphere in Italy*, pp. 157–176, eds Boriani, A., Bonafede, M., Piccardo, G. B. & Vai, G. B., Accademia Nazionale dei Lincei, Rome, Italy.

Philip, H., 1987. Plio-Quaternary evolution of the stress field in Mediterranean zones of subduction and collision, *Ann. Geophys.*, **5B**, 301–320.

Reasenber, P.A. & Oppenheimer, D., 1985. Fortran computer

- programs for calculating and displaying earthquake fault-plane solutions, *USGS Open File Rept*, No. 85-739.
- Ritsema, A., 1979. Active or passive subduction at the Calabrian arc, *Geol. Mijn.*, **58**, 127–134.
- Rothè, J.P., 1969. *The seismicity of the Earth 1953–1965*, UNESCO, Paris.
- Royden, L.R., 1993. Evolution of retreating subduction boundaries formed during continental collision, *Tectonics*, **12**, 629–638.
- Royden, L., Patacca, E. & Scandone, P., 1987. Segmentation and configuration of subducted lithosphere in Italy: an important control on thrust-belt and foredeep-basin evolution, *Geology*, **15**, 714–717.
- Selvaggi, G. & Chiarabba, C., 1995. Seismicity and *P*-wave velocity image of the Southern Tyrrhenian subduction zone, *Geophys. J. Int.*, **121**, 818–826.
- Spakman, W., 1988. Upper mantle delay time tomography, *PhD thesis*, University of Utrecht, Utrecht, The Netherlands.
- Spakman, W., van der Lee, S. & van der Hilst, R., 1993. Travel-time tomography of the European-Mediterranean mantle down to 1400 km, *Phys. Earth planet. Inter.*, **79**, 3–74.
- Vassiliou, M.S., 1984. The state of stress in subducting slabs as revealed by earthquakes analysed by moment tensor inversion, *Earth planet. Sci. Lett.*, **69**, 195–202.
- Vassiliou, M.S. & Hager, B.H., 1988. Subduction zone earthquakes and stress in slabs, *Pageoph*, **128**, 547–624.
- Vassiliou, M.S., Hager, B.H. & Raefsky, A., 1984. The distribution of earthquakes with depth and stress in subducting slabs, *J. Geodyn.*, **1**, 11–28.
- Westaway, R., 1993. Quaternary uplift of southern Italy, *J. geophys. Res.*, **98**, 21 741–21 772.
- Wortel, M.J.R. & Spakman, W., 1992. Structure and dynamics of subducted lithosphere in the Mediterranean region, *Proc. Kon. Ned. Akad. v. Wetensch.*, **95**, 325–347.
- Zhou, H., 1990. Observations on earthquake stress axes and seismic morphology of deep slabs, *Geophys. J. Int.*, **103**, 377–401.